Accurate Estimation of Microtubule Dynamics using Kymographs and Variable-Rate Particle Filters

Ihor Smal, Ilya Grigoriev, Anna Akhmanova, Wiro J. Niessen, Erik Meijering

Abstract— **Studying intracellular dynamics is of major importance for understanding healthy life at the molecular level and for developing drugs to target disease processes. One of the key technologies to enable this research is the automated tracking and motion analysis of subcellular objects in microscopy image sequences. Contrary to common frame-by-frame tracking methods, two alternative approaches have been proposed recently, based on either Bayesian estimation or space-time segmentation, which better exploit the available spatiotemporal information. In this paper, we propose to combine the power of both approaches, and develop a new probabilistic method to segment the traces of the moving objects in kymograph representations of the image data. It is based on variable-rate particle filtering and uses multiscale trend analysis for estimation of the relevant kinematic parameters using the extracted traces. Experiments on realistic synthetically generated images as well as on real biological image data demonstrate the improved potential of the new method for the analysis of microtubule dynamics *in vitro*.**

I. INTRODUCTION

Subcellular motion analysis plays a major role in understanding fundamental dynamical processes occurring in biological cells. Even though many intracellular interaction mechanisms are well understood these days, many questions still remain unanswered. In some cases, where the analysis in living cells (*in vivo*) is confounded by other intracellular processes, it makes sense to study the intracellular dynamics *in vitro*, where the influence of other structures or processes is removed, reduced, or known [1], [2].

Nowadays, intracellular dynamics is usually visualized using advanced fluorescence microscopy imaging techniques, where the objects of interest are labeled with fluorescent proteins [3], [4]. Alternatively, non-fluorescence based techniques, such as phase contrast (PC) or differential interference contrast (DIC) microscopy can sometimes be used, which do not require labeling [3]. In either case, the optical resolution of the microscope is much lower (on the order of 100 nm) than the size of the objects of interest (on the order of nanometers), causing the latter to be imaged as blurred spots due to diffraction. The quality of the images is further reduced by high levels of measurement noise [4]. Both types of distortions contribute to the ambiguity of the data, making automated quantitative image analysis very difficult.

This work was financially supported by the Netherlands Organization for Scientific Research (NWO) through VIDI-grant 639.022.401.

I. Smal, W. J. Niessen, and E. Meijering are with the Biomedical Imaging Group Rotterdam, Departments of Medical Informatics and Radiology, Erasmus MC, Rotterdam, The Netherlands.

I. Grigoriev and A. Akhmanova are with the Department of Cell Biology, Erasmus MC, Rotterdam, The Netherlands.

In time-lapse microscopy, where hundreds to thousands of 2D or 3D images are acquired sequentially in time, the main task is to track the objects of interest (proteins, vesicles, microtubules, etc.) and compute relevant motion parameters from the extracted trajectories. In practice, manual tracking is labor intensive and poorly reproducible, and only a small fraction of the data can be analyzed this way. The vast majority of automatic tracking methods [5]–[8] developed in this field consist of two stages: *detection* of objects of interest (independently in each frame), and *linking* of detected objects from frame to frame (solving the correspondence problem). Since the methods employed for the first stage operate on data with low signal-to-noise ratio (SNR), the linking procedure in the second stage is faced with either many false positives (noise classified as objects) or false negatives (misdetection of actually present objects).

Contrary to these two-stage tracking methods, which typically use only very few neighboring frames to address the correspondence problem, methods that make better use of the available temporal information usually show better results. Such trackers are either built within a Bayesian framework [9], which in any frame uses all available temporal information up to that frame, or they consider the 2D+t or 3D+t image data as one spatiotemporal 3D or 4D image, respectively, and translate the estimation of trajectories into a segmentation of spatiotemporal structures [10].

In this paper, we propose to combine the power of the latter two approaches, and develop a variable-rate particle filtering method that implements the idea of Bayesian estimation for tracing spatiotemporal structures formed by transforming the original time-lapse microscopy image data into a special type of spatiotemporal representation: kymographs [11]. This novel, combined approach results in more accurate extraction of the spatiotemporal structures (edge-like image structures in our case) compared to particle filtering applied directly to the image sequences on a per-frame basis [9].

II. METHODS

A. Microtubule Dynamics

Microtubules (MTs) are polarized tubular filaments (diameter $\sim$25 nm) composed of α/β-tubulin heterodimers that play a major role in several intracellular processes such as cell division, internal cell organization, and intracellular transport. To understand the specific interactions between regulatory proteins and microtubules is of great interest to biologists. Misregulation of MT dynamics, for example, can lead to erroneous mitosis, which is a characteristic feature in neurodegenerative diseases.

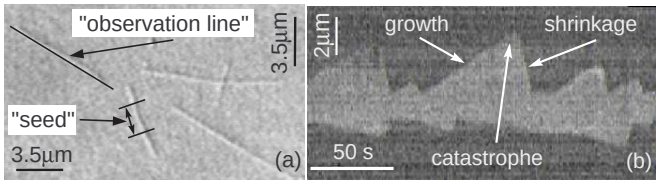

Fig. 1. (a) Example of a DIC microscopy image. Microtubule nucleation initiates from stable tubulin "seeds". In the experiments, "observation lines" are drawn along MT bodies to construct kymographs. (b) Example of a kymograph obtained from the DIC microscopy images, showing the dynamics of both MT ends.

The dynamics of MTs is highly regulated, both spatially and temporally, by a wide family of MT associated proteins (MAPs) [12]. MTs frequently switch between growth and shrinkage, a feature called dynamic instability [13]. Growth and shrinkage proceed with nearly constant velocities, where the shrinkage velocity, ν^-, is usually much higher than the growth velocity ν^+. The growth velocity *in vivo* can be up to 10 times faster than *in vitro*. Two other important events that characterize dynamic instability are *rescue* (switching from shrinkage to growth) and *catastrophe* (switching from growth to shrinkage) [13]. In practice, the analysis of MT dynamics includes estimation of ν^+, ν^-, and the rescue and catastrophe frequencies, f_{res} and f_{cat}.

Recent studies reveal a special class of MAPs, plus-end-tracking proteins (+TIPs), that are able to accumulate at MT growing ends [12]. One way to understand the mechanism employed by individual +TIPs and the molecular mechanisms underlying their functions is by measuring the distribution and displacement of +TIPs in time. *In vivo*, it is extremely hard to decouple the effect of other regulators while studying +TIPs influence on MT dynamics. The advantage of *in vitro* investigation is the minimal environment in which the influence of various +TIPs can be dissected individually. However, due to lack of robust and accurate automatic methods, the manual analysis usually is a labor intensive procedure which very likely leads to user bias and loss of important information.

B. Imaging Technique and Kymographs

In our studies, the dynamic behavior of MTs is imaged using DIC microscopy [3], [4], which is effectively used for biological specimens that cannot be visualized with sufficient contrast using bright-field microscopy. The resulting images (see Fig. 1(a) for an example) depict objects as black/white shadows on a gray background with good resolution and clarity. The advantages of DIC over fluorescence microscopy is that the samples do not have to be stained. As a result, the possible influence of fluorescent proteins is also eliminated. The main limitation of this imaging technique is its requirement for a thin and transparent sample of fairly similar refractive index to its surroundings.

Automatic analysis of MT behavior *in vitro* using time-lapse DIC microscopy requires tracking of the plus-end of each MT so as to obtain 2D paths in the image plane, from which the parameters of interest (velocity and frequency estimates) can be computed. This is hampered by the usually poor image quality, caused by high (Poisson) noise levels, blurring of the subresolution MT-structures, and the nonlinear image formation process in DIC microscopy, as a result of which the objects (especially the MT tips) cannot be easily modeled by appearance models, as in the case of fluorescence microscopy imaging [9].

To better exploit the temporal information in the data, contrary to direct frame-by-frame tracking, we propose to base the motion parameter estimation on a transformation of the data that is more amenable to multiscale analysis. Specifically, we propose to use a kymograph representation [11] for each MT, constructed by defining (manually or automatically) an "observation line" L (Fig. 1(a)) in the image sequence along the MT body. Image intensity values are then sampled equidistantly along L, yielding a vector of "measurements" at time t, $J_t = \{J_t(j) : j = 1, \ldots, Y\}$, where Y is the number of samples for the selected MT in every image frame. The resulting kymograph (see Fig. 1(b) for an example), $I(t, y) = \{J_t : t = 1, \ldots, T\}$, is the collection of measurement vectors, where every column t contains the measurements J_t as pixel values, and T is the number of frames in the image sequence.

To estimate the kinematic parameters of interest from the kymographs, the edge location $y(t)$ (corresponding to the MT tip) must be accurately extracted. Since the instant velocity ν at any time t' is estimated as $\nu = (dy/dt)_{t=t'} = \tan(\varphi)$, with φ the angle between the time axis and the tangent to $y(t)$ at $t = t'$, small errors in the angle estimates may lead to large velocity estimation errors (and due to the nonlinearity of the tangent, the closer φ is to 90 degrees, the larger the errors). Here, frequently used edge detectors such as the gradient magnitude or Canny's method produce unsatisfactory results (see also Fig. 2(b)), due to noise amplification (by differentiation) or edge blurring (by regularization). Instead, we propose to use edge model fitting using particle filtering (PF) methods [14]. The PF can be exploited to reduce the overload of fitting the model in every pixel position, by incorporating information about the edge model, the image noise distribution, and the probability of finding the edge in the neighborhood of a pixel.

C. Variable-Rate Particle Filtering

Particle filters implement the concept of Bayesian estimation, where at each time t a system state $\mathbf{x}_t$ is estimated from previous states, noisy measurements $\mathbf{z}_t$, and prior knowledge about the underlying processes in terms of probability density functions (pdf): the state transition $p(\mathbf{x}_t|\mathbf{x}_{t-1})$ and the observation model $p(\mathbf{z}_t|\mathbf{x}_t)$ [14]. The solution to the state estimation problem is the posterior pdf $p(\mathbf{x}_{0:t}|\mathbf{z}_{0:t})$, where $\mathbf{x}_{0:t} = \{\mathbf{x}_0, \ldots, \mathbf{x}_t\}$ and $\mathbf{z}_{0:t} = \{\mathbf{z}_0, \ldots, \mathbf{z}_t\}$, which in general can be found using sequential Monte Carlo (MC) methods [14], where the posterior pdf is approximated with a set of N_s MC samples ("particles"), $\{\mathbf{x}_{0:t}^{(i)}, w_t^{(i)}\}_{i=1}^{N_s}$, as $p(\mathbf{x}_{0:t}|\mathbf{z}_{0:t}) = \sum_{i=1}^{N_s} w_t^{(i)} \delta(\mathbf{x}_{0:t} - \mathbf{x}_{0:t}^{(i)})$. Each $\mathbf{x}_{0:t}^{(i)}$ describes a possible state sequence (path) and the weight $w_t^{(i)}$ indicates the path probability. The solution using PF is given by a recursive procedure that predicts the state

from time $t-1$ to t and updates the weights based on newly arrived measurements $\mathbf{z}_t$ as

$$\mathbf{x}_t^{(i)} \sim p(\mathbf{x}_t|\mathbf{x}_{t-1}^{(i)}) \text{ and } w_t^{(i)} \propto w_{t-1}^{(i)} p(\mathbf{z}_t|\mathbf{x}_t^{(i)}), \quad (1)$$

$i = 1, \ldots, N_s$. The minimum mean square error (MMSE) or maximum a posteriori (MAP) estimators of the state can be easily obtained from $p(\mathbf{x}_{0:t}|\mathbf{z}_{0:t})$ [14].

Commonly, the state sampling rate is determined by the rate at which the measurements arrive. In our application, however, the MT dynamics is characterized by prolonged periods of smoothness (growth or shrinkage) with infrequent sharp changes (rescue or catastrophe). This allows a much more parsimonious representation of the MT tip trajectory: more state points are allocated in regions of rapid change and relatively fewer points in smoother sections. This data-adaptive state sampling is possible using recently introduced variable-rate particle filtering (VRPF) [15]. Within the VRPF framework, the state is defined as $\mathbf{x}_k = (\theta_k, \tau_k)$, where $k \in \mathbb{N}$ is a discrete state index, $\tau_k \in \mathbb{R}^+ > \tau_{k-1}$ is the arrival time for the state k, and θ_k is the vector of variables necessary to parametrize the object state. In tracking applications, θ_k may include position, velocity, heading, etc. In our case, we define $\theta_k = (y_k, v_k)$, where y_k is the edge position at time τ_k along the observation line L, and $v_k = (dy/dt)_{t=\tau_k}$ describes the edge direction at $t = \tau_k$ in the image $I(t, y)$. Similar to standard PF, the state sequence is assumed to be a Markov process, so the successive states are independently generated with increasing k according to

$$\mathbf{x}_k \sim p(\mathbf{x}_k|\mathbf{x}_{k-1}) = p_\theta(\theta_k|\theta_{k-1}, \tau_k, \tau_{k-1}) p_\tau(\tau_k|\theta_{k-1}, \tau_{k-1}).$$

In our implementation, the states $\mathbf{x}_k$ for the prediction-update procedure (1) are sampled as

$$\tau_k - \tau_{k-1} \sim \mathcal{U}_{[\tau^0, \tau^1]}, \qquad v_k \sim p(v_k|v_{k-1}), \quad (2)$$

and $y_k = y_{k-1} + v_{k-1}(\tau_k - \tau_{k-1})$, where $\mathcal{U}_{[a,b]}$ denotes the uniform distribution in the range $[a, b]$. The sampling of the new states $\mathbf{x}_k$ at time t is performed only for those particles $\mathbf{x}_{k-1}^{(i)}$ for which $\tau_{k-1}^{(i)} \leq t$, which also reduces the computational load compared to the standard PF implementation.

The crucial point in applying the VRPF framework is to efficiently model the prior $p(v_k|v_{k-1})$ to catch the rapid changes in edge orientation. Considering three possible motion types (growth, shrinkage, no activity), we define the following prior for the velocity component v_k:

$$p(v_k|v_{k-1}) = \begin{cases} (1-a)\mathcal{N}(v_{k-1}, \sigma_{\nu^+}^2) + a\mathcal{N}(\nu^-, \sigma_{\nu^-}^2) & \text{for } v_{k-1} > V_{\text{th}}, \\ (1-a)\mathcal{N}(v_{k-1}, \sigma_{\nu^-}^2) + & \\ \quad \frac{a}{2}\left(\mathcal{N}(\nu^+, \sigma_{\nu^+}^2) + \mathcal{N}(0, \sigma_{\nu^0}^2)\right) & \text{for } v_{k-1} < -V_{\text{th}}, \\ (1-a)\mathcal{N}(v_{k-1}, \sigma_{\nu^+}^2) + a\mathcal{N}(\nu^+, \sigma_{\nu^+}^2) & \text{for } |v_{k-1}| < V_{\text{th}}, \end{cases}$$

where $0 < a < 1$ is a weighting parameter that balances the mixture components corresponding to the different types of motion in the transition pdf (in tracking applications, a corresponds to the probability of object/target birth). The variances for the velocity estimates ($\sigma_{\nu^+}^2$, $\sigma_{\nu^-}^2$, $\sigma_{\nu^0}^2$) account for possible small deviations in the measured velocities from the average values. The thresholding at V_{th} determines which prior is used but does not imply that at every time point we assume that the system evolves according to only one motion model. Due to the probabilistic nature of the VRPF, at every time step the posterior pdf describes the probability to find the MT in each of the three states.

To measure the likelihood of edge existence at some image position, with the orientation defined by the velocity component v_{k-1} of the state vector, average intensity values are computed for both (black and white) rectangles (see Fig. 2), μ_B and μ_F, corresponding to the background and foreground intensities. The likelihood is defined as $p(\mathbf{z}_t|\mathbf{x}_{k-1}, \mathbf{x}_k) \propto \exp(\mu_F - \mu_B)$, if $\mu_F - \mu_B > 0$ and is zero otherwise, where $\tau_{k-1} \leq t < \tau_k$. It means that sharp edges are favored over smoother noisy intensity transitions. The width d, which also controls the sensitivity of the observation model to the edge location, should be specified. The length $l_v = (\tau_k - \tau_{k-1})\sqrt{1 + v_{k-1}^2}$ is automatically defined by the time sampling functions (2). The variety of l_v caused by the sampling (2) adds some multiresolution property to the analysis because the edge presence at some image point is now analyzed on several different scales.

In order to derive the MMSE estimator, the principle of fixed-lag smoothing is used, where the estimation of the edge position at time t is delayed until the measurements at time $t + \Delta t$ will be processed and the posterior updated, which greatly improves the final results.

D. Multiscale Trend Analysis

Having the estimated edge $\hat{y}_t$ after applying the VRPF, we employ multiscale trend analysis (MTA) [16] in order to automatically compute all the parameters of interest. At this stage of our analysis, it is necessary to detect all the catastrophe and rescue events and split the live history $\hat{y}_t$ into parts of growth and shrinkage, possibly separated by stages of no activity.

III. EXPERIMENTAL RESULTS

A. Evaluation on Synthetic Data

The performance of the proposed VRPF-based method was evaluated using synthetic images as well as real data showing MT dynamics *in vitro*. The synthetically generated images (see Fig. 2(a)) enabled us to explore the accuracy and robustness of the method depending on the image quality (different SNR levels) and the parameter values that model the MT dynamics. The proposed VRPF method was evaluated using 20 synthetically generated images, where the ground truth values were fixed to $\nu^0 = 0$, $\nu^+ = 0.5$, $\nu^- = -3$, $\sigma_{\nu^0}^2 = \sigma_{\nu^-}^2 = \sigma_{\nu^+}^2 = 0.005$, and $f_{\text{res}} = 0.018$, $f_{\text{cat}} = 0.009$, which are representative of real data. The velocity estimates are given in pixels/frame. Since the ground truth was available in these experiments, the accuracy of extracting the edges was evaluated using the root mean square error (RMSE). The results of applying MTA for kinematic parameter estimation based on the edges extracted using the VRPF are shown in Table I.

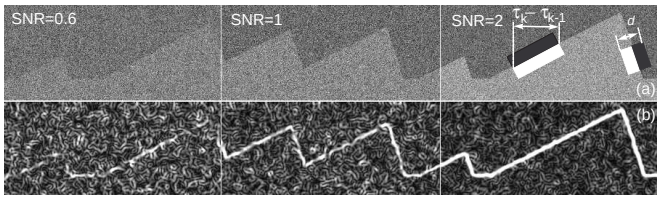

Fig. 2. Examples of the synthetic images for different SNR levels used in the experiments (a), for which the gradient images (b) are computed using Gaussian derivatives at a smoothing scale of 3 pixels.

TABLE I

RESULTS OF PARAMETER ESTIMATION USING THE VRPF AND MTA.

SNR	RMSE	$\nu^+ \pm$ sd	$\nu^- \pm$ sd	f_{cat}	f_{res}
0.4	2.54	0.47±0.07	-2.41±0.79	0.011	0.019
0.6	1.43	0.50±0.03	-3.03±0.61	0.009	0.018
0.8	1.23	0.49±0.02	-2.91±0.62	0.009	0.017
1.0	1.15	0.50±0.01	-2.96±0.37	0.009	0.017

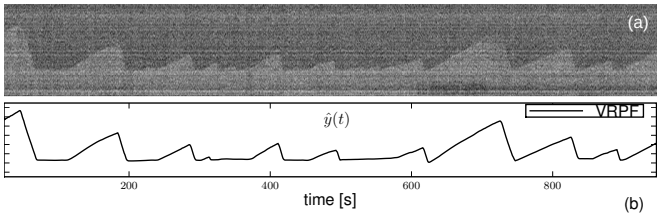

Fig. 3. Example of a kymograph generated in the experiments on real DIC microscopy image data with SNR ≈ 1 (a) and the results of applying the proposed VRPF (b).

B. Evaluation on Real Data

For the validation on real data we collected three representative DIC microscopy image sequences acquired to study the influence of different concentrations of EB3 (end-binding protein 3) and GFP-EB3 (EB3 fused to the green fluorescent protein) on the MT growth and shrinkage velocities (ν^+ and ν^-) and the catastrophe rate (f_{cat}). The sequences were taken from experiments with MT nucleation from stable tubulin seeds, where 15μM of tubulin was added (Experiment I), or, in addition, 1μM of EB3 (Experiment II), or 1μM of GFP-EB3 (Experiment III) [2]. They consisted of about 1000-1200 frames (one per second) of size 700×500 pixels (of size 86×86 nm^2). To estimate the parameters of interest, for each experiment 10 kymographs were constructed and analyzed manually and using the proposed VRPF method. An example of edge extraction using VRPF in real data is shown in Fig. 3. The obtained estimates (ν^+, ν^-, f_{cat}) for Experiment I (0.51μm/min, -9.72μm/min, 0.002), Experiment II (2.52μm/min, -14.65μm/min, 0.014), and Experiment III (2.58μm/min, -14.03μm/min, 0.014) are in agreement with recently published results [2] obtained manually.

IV. CONCLUSIONS

In this paper we have proposed a novel approach for the automatic analysis of microtubule dynamics *in vitro* imaged using time-lapse DIC microscopy. The task of tracking microtubule tips on a per-frame basis in the noisy images is replaced by segmentation of spatiotemporal structures (edges in our case) in space-time images (kymographs). For the extraction of these structures from the kymographs and estimation of the important kinematic parameters, we have proposed a variable-rate particle filtering method, which is built within a Bayesian framework and optimally combines the measurements and prior knowledge about the underlying processes, in combination with subsequent multiscale trend analysis. The results of quantitative evaluation of the proposed method in realistic synthetic images as well as in real biological data demonstrate that the method is capable of accurate estimation of the parameters characterizing microtubule dynamics and suggest that the method may replace laborious manual procedures.

REFERENCES

[1] E. L. Munteanu, "Dynamics and regulation at the tip: A high resolution view on microtubule assembly," Ph.D. dissertation, Institute for Atomic and Molecular Physics (AMOLF), Amsterdam, 2008.

[2] Y. Komarova, C. O. de Groot, I. Grigoriev, S. M. Gouveia, E. L. Munteanu, J. M. Schober, S. Honnappa, R. M. Buey, C. C. Hoogenraad, M. Dogterom, G. G. Borisy, M. O. Steinmetz, and A. Akhmanova, "Mammalian end binding proteins control persistent microtubule growth," *Journal of Cell Biology*, vol. 184, pp. 691–706, 2009.

[3] D. J. Stephens and V. J. Allan, "Light microscopy techniques for live cell imaging," *Science*, vol. 300, no. 5616, pp. 82–86, 2003.

[4] Q. Wu, F. A. Merchant, and K. R. Castleman, *Microscope Image Processing*. Burlington, MA: Elsevier Academic Press, 2008.

[5] D. Thomann, D. R. Rines, P. K. Sorger, and G. Danuser, "Automatic fluorescent tag detection in 3D with super-resolution: Application to the analysis of chromosome movement," *Journal of Microscopy*, vol. 208, no. 1, pp. 49–64, 2002.

[6] A. Genovesio, T. Liedl, V. Emiliani, W. J. Parak, M. Coppey-Moisan, and J.-C. Olivo-Marin, "Multiple particle tracking in 3-D+t microscopy: Method and application to the tracking of endocytosed quantum dots," *IEEE Transactions on Image Processing*, vol. 15, no. 5, pp. 1062–1070, 2006.

[7] K. Jaqaman, D. Loerke, M. Mettlen, H. Kuwata, S. Grinstein, S. Schmid, and G. Danuser, "Robust single-particle tracking in live-cell time-lapse sequences," *Nature Methods*, vol. 5, no. 8, pp. 695–702, 2008.

[8] E. Meijering, I. Smal, and G. Danuser, "Tracking in molecular bioimaging," *IEEE Signal Processing Magazine*, vol. 23, no. 3, pp. 46–53, 2006.

[9] I. Smal, K. Draegestein, N. Galjart, W. Niessen, and E. Meijering, "Particle filtering for multiple object tracking in dynamic fluorescence microscopy images: Application to microtubule growth analysis," *IEEE Transactions on Medical Imaging*, vol. 27, no. 6, pp. 789–804, 2008.

[10] S. Bonneau, M. Dahan, and L. D. Cohen, "Single quantum dot tracking based on perceptual grouping using minimal paths in a spatiotemporal volume," *IEEE Transactions on Image Processing*, vol. 14, no. 9, pp. 1384–1395, 2005.

[11] B. Hinz, W. Alt, C. Johnen, V. Herzog, and H.-W. Kaiser, "Quantifying lamella dynamics of cultured cells by SACED, a new computer-assisted motion analysis," *Experimental Cell Research*, vol. 251, pp. 234–243, 1999.

[12] A. Akhmanova and M. O. Steinmetz, "Tracking the ends: a dynamic protein network controls the fate of microtubule tips," *Nature Reviews Molecular Cell Biology*, vol. 9, no. 4, pp. 309–322, 2008.

[13] T. Mitchison and M. Kirschner, "Dynamic instability of microtubule growth," *Nature*, vol. 312, no. 5991, pp. 237–242, 1984.

[14] S. M. Arulampalam, S. Maskell, N. Gordon, and T. Clapp, "A tutorial on particle filters for online nonlinear/non-Gaussian Bayesian tracking," *IEEE Transactions on Signal Processing*, vol. 50, no. 2, pp. 174–188, 2002.

[15] S. Godsill and J. Vermaak, "Variable rate particle filters for tracking applications," in *Proceedings of the IEEE/SP 13th Workshop on Statistical Signal Processing*, 2005, pp. 1280–1285.

[16] I. Zaliapin, I. Semenova, A. Kashina, and V. Rodionov, "Multiscale trend analysis of microtubule transport in melanophores," *Biophysical Journal*, vol. 88, pp. 4008–4016, 2005.